Frontiers in Bioscience Landmark

Front. Biosci. (Landmark Ed) **2025**; 30(3): 28260
https://doi.org/10.31083/FBL28260

Original Research

Comparative Study of Structural and Functional Rearrangements in Skeletal Muscle Mitochondria of SOD1-G93A Transgenic Mice at Pre-, Early-, and Late-Symptomatic Stages of ALS Progression

Natalia V. Belosludtseva[1,*], Anna I. Ilzorkina[1], Mikhail V. Dubinin[2], Irina B. Mikheeva[1], Konstantin N. Belosludtsev[1]

[1]Institute of Theoretical and Experimental Biophysics, Russian Academy of Sciences, 142290 Pushchino, Russia
[2]Department of Biochemistry, Cell Biology and Microbiology, Mari State University, 424001 Yoshkar-Ola, Russia
*Correspondence: belosludtsevanv@iteb.pushchino.ru (Natalia V. Belosludtseva)
Academic Editor: Gianluca Paventi
Submitted: 16 November 2024 Revised: 23 January 2025 Accepted: 30 January 2025 Published: 18 March 2025

Abstract

Background: Amyotrophic lateral sclerosis (ALS) is a progressive multisystem disease characterized by limb and trunk muscle weakness that is attributed, in part, to abnormalities in mitochondrial ultrastructure and impaired mitochondrial functions. This study investigated the time course of structural and functional rearrangements in skeletal muscle mitochondria in combination with motor impairments in Tg (copper-zinc superoxide dismutase enzyme (SOD1) G93A) dl1/GurJ (referred to as SOD1-G93A/low) male mice, a familial ALS model, as compared with non-transgenic littermates. **Methods**: The neurological status and motor functions were assessed weekly using the paw grip endurance method and the grid suspension test with two-limb and four-limb suspension tasks. Transmission electron microscopy followed by quantitative analysis was performed to study ultrastructural alterations in the quadriceps femoris. Functional analysis of skeletal muscle mitochondria was performed using high-resolution Oxygraph-2k (O2K) respirometry and methods for assessing the calcium retention capacity index and the content of lipid peroxidation products in freshly isolated preparations. **Results**: Based on the behavioral phenotyping data, specific age groups were identified: postnatal day 56 (P56) (n = 10–11), 84 (P84) (n = 10–11), and 156 (P154) (n = 10–12), representing the pre-symptomatic, early-symptomatic and late-symptomatic stages of ALS progression in SOD1-G93A/low mice, respectively. Electron microscopy showed mosaic destructive changes in subsarcolemmal mitochondria in fibers of the quadriceps femoris from 84-day-old SOD1-G93A/low mice. Morphometric analysis revealed an elevation in the mean size of the mitochondria in SOD1-G93A mice at P84 and P154. In addition, the P154 transgenic group demonstrated a decrease in sarcomere width and the number of mitochondria per unit area. At the symptomatic stage, SOD1-G93A mice exhibited a decreased respiratory control ratio, ADP-stimulated, and uncoupled respiration rates of mitochondria isolated from the quadriceps femoris muscle, as measured by high-resolution respirometry. In parallel, the mitochondria showed lower calcium retention capacity and increased levels of lipid peroxidation products compared with the control. **Conclusions**: Taken together, these results indicate stage-dependent changes in skeletal muscle mitochondrial ultrastructure and functions associated with defective oxidative phosphorylation, impaired calcium homeostasis, and oxidative damage in the SOD1-G93A/low mouse model, which appears to be a promising direction for the development of combination therapies for ALS.

Keywords: ALS; mouse SOD1*G93A model; behavioral phenotyping; pre-symptomatic stage; symptomatic stage; skeletal muscle mitochondria; ultrastructure; mitochondrial function; calcium retention capacity; lipid peroxidation

1. Introduction

Amyotrophic lateral sclerosis (ALS) is a progressive motor neuron disease that causes extreme weakness and atrophy of trunk and limb muscles both in patients and transgenic animal models [1,2]. The pathology presents both with spastic paralysis in the lower limbs and flaccid paralysis in the upper limbs, suggesting the disruption of the upper and lower motor pathways [2]. Beginning with focal muscle weakness, the disease progresses to weakness of most skeletal muscles without loss of sensation, and ultimately leads to death.

ALS is a multifactorial disease associated with a genetic predisposition (familial (f) form), with a large (12–23%) subgroup carrying different variants in the gene encoding the copper-zinc superoxide dismutase enzyme (SOD1), and/or is provoked by a number of adverse environmental factors (sporadic (s) form), including strenuous physical activity, severe emotional stress, long-term exposure to inorganic metalloids, etc., [1,3,4]. In both forms, the pathological features and clinical symptoms of ALS have been reported to be the same. The incidence rate for ALS overall climbs steadily as age increases, and the prevalence according to the latest World Health Organization (WHO) data is 3.9–5.0 per 100,000 population [5]. Pathogenetic mechanisms, especially those that initiate degenerative events in muscle tissues, are unclear, and therefore there are still no effective treatments for this disease.

From a neurocentric perspective, skeletal muscle weakness results from the degeneration of upper motor neurons in the cerebral cortex and lower motor neurons in the spinal cord and brainstem [6]. Recently, this point of view has been challenged by the finding of early changes in skeletal muscle function without concomitant motor neuron axonal retraction in ALS patients and animal models, indicating mechanisms of "dying back" or slowly evolving neurodegeneration in a distal-to-proximal direction [7–9]. Accumulating evidence has shown that skeletal muscle is an important target tissue in ALS, with dysfunction resulting from intracellular disturbances at multiple levels, including energy metabolism, RNA processing, satellite cell activity, and mitochondrial function [9].

It is widely acknowledged that skeletal muscle is about 45% of body mass and provides approximately 30% of resting energy expenditure [10]. Mitochondria are pivotal organelles responsible for regulating the metabolic status, guiding aerobic ATP synthesis, controlling muscle mass and susceptibility to apoptosis, maintaining redox and ion homeostasis in skeletal muscle. These organelles occupy 6–8% of muscle fiber volume and largely determine its metabolic flexibility in order to meet the requirements under ever changing pathophysiological conditions [10–12]. Of note, mitochondria are found to cluster between myofibrils, near the nucleus, and underneath the sarcolemmal membrane of skeletal myocytes. In the case of subsarcolemmal location, mitochondria may be exposed to higher calcium concentrations and display more pronounced functional variations within affected muscle fibers [11,13]. In pathological conditions, mitochondrial dysfunction may be caused by ultrastructural alterations, defective oxidative phosphorylation, ion dyshomeostasis, mainly disbalanced calcium concentration, and redox imbalance [11].

Although ALS-related mitochondrial abnormalities have been investigated in much greater detail for motor neurons, they have also been identified in skeletal muscle cells in various models and patients [14,15]. Accumulating evidence indicates impaired mitochondrial bioenergetics in muscle biopsy specimens from affected individuals both with fALS and sALS [16]. Studies using SOD1 transgenic mice, a classical fALS animal model, have reported that skeletal muscle mitochondria exhibit altered structure and calcium handling, reduced mitochondrial DNA and oxidative phosphorylation, and elevated pool of reactive oxygen molecules [17]. Some *in vitro* studies have reported that mutant forms of the SOD1 enzyme can accumulate directly in the intermembrane space and matrix of these organelles, causing disturbances in their ultrastructure and functions [15,17,18]. In contrast, the overall loss of intact enzyme activity in CuZnSOD knockout (*Sod1*$^{-/-}$) mice, specific to muscle tissue, does not lead to mitochondria dysfunction and significant muscle atrophy, suggesting a direct significance of the gained function of *SOD1* mutations at the onset of ALS [4,17,19]. However, data on abnormalities in the morphology and functions of mitochondria, taking into account their progression and topography in affected skeletal muscle fibers upon SOD1-associated ALS, are still scarce and controversial.

In this study, we comprehensively characterized structural and functional rearrangements in skeletal muscle mitochondria in association with motor symptoms in transgenic male B6SJLTg (SOD1-G93A) dl1Gur/J (referred to as SOD1-G93A/low) mice at three time points on the postnatal (P) days P56, P84, and P154, in comparison with those in non-transgenic age-matched animals. Specific age groups of SOD1-G93A animals were established based on the results of weekly measurements of neurological status and motor function using two behavioral tests: the paw grip endurance (string) test and grid suspension test with two-limb and four-limb suspension tasks. The study revealed the time course of mitochondrial abnormalities in the quadriceps femoris muscle of SOD1 transgenic mice from the age groups P56, P84, and P154, which can be attributed to the presymptomatic, early and late symptomatic stages of ALS severity and progression.

2. Materials and Methods

2.1 SOD1-G93A Mouse Model

Specific pathogen-free mice (males) of the congenic line B6SJLTg (SOD1-G93A) dl1Gur/J (SOD1-G93A) (The Jackson Laboratory, Bar Harbor, ME, USA) expressing a variant of the human *SOD1* gene with a substitution of glycine to alanine at position 93 (G93A) in all tissues (n = 30) were used. The low expressor mutant SOD1-G93A transgenic mice develop a delayed phenotype due to a persistent reduction in the number of transgene copies and are characterized by paralytic disorders and muscle deficits, as in human ALS [20–22]. As a control phenotype, littermates of the same sex that did not inherit the mutant *SOD1* gene (non-transgenic mice) (n = 34) were employed. In total, 64 experimental mice at six weeks of age were purchased from the accredited Institute of Bioorganic Chemistry (IBCh) animal breeding facility (the Unique Research Unit Bio-Model of the Branch of the Shemyakin and Ovchinnikov Institute of Bioorganic Chemistry, Russian Academy of Sciences, Pushchino, Russia; agreement #2850/22-T(UNU) dated 01/23/2023) and housed within the animal facility at the Theoretical and Experimental Biophysics of RAS (Pushchino, Russia). SOD1-G93A and non-transgenic male mice were maintained in a controlled environment (24 $\pm$ 1 °C) under a normal 12/12-h dark/light cycle with continuous access to drinking water and food. The use of mice of one (male) sex in this study eliminates the influence of hormonal cycles and ensures standardized age-related responses.

All protocols with experimental mice were approved by the Biosafety and Bioethics Committee (permission No. 02/2023 dated February 08, 2023) of the Institute of Theoretical and Experimental Biophysics of RAS. Experimental

animals received humane care in accordance with the Rules for Conducting Research with Experimental Animals (Order of the Ministry of Health of Russia dated August 12, 1997 No. 755) and the Principles of Laboratory Animal Care proclaimed by the Directive 2010/63/EC of the European Parliament. At the end of the observation period, the experimental animals were sacrificed by cervical dislocation under anesthesia with a mixture of 40 mg/kg zoletil (Valdepharm, Val-de-Reuil, France) and 10 mg/kg xylazine (Bioveta, Ivanovice na Hane, Czech Republic).

2.2 Behavioral Phenotype Testing of Experimental Mice

Monitoring of the behavioral phenotype of mice was carried out twice a week according to the phenotypic screening protocol that includes a robust neurological scoring system designed by the ALS Therapy Development Institute (ALS TDI) [23]. This scoring system focuses primarily on the assessment of hindlimb deficits as the earliest documented neurological feature in SOD1-G93A animals. According to this system, NS 1 and NS 2 indicate that the mouse's hind limbs are partially or completely paralyzed, respectively. NS 0 is considered the "normal" phenotype. At the start of behavioral phenotype testing, the age of mice was 42 days ($\pm$ 3 days). The dynamics of animal weight were calculated as a percentage. The weight of experimental mice at P42 was taken as 100%, which was 19.2 $\pm$ 0.5 g and 19.6 $\pm$ 0.3 g for the non-Tg and SOD1-G93A groups, respectively.

The motor performance of the experimental mice from 42nd to 154th day after birth was estimated once a week using the string test ("paw grip endurance test" or "wire hanging test") and the grip strength test (IITC Life Science, Woodland Hills, CA, USA). In the paw grip endurance test, each animal was put on a 38 cm long 3 mm wire, located 50 cm above the covered surface to soften the mouse's fall. The time (s) that a mouse can hang for was recorded to assess locomotor abnormalities. The grip strength measurement test was used to evaluate forelimb (2 paws) and fore-/hindlimb (4 paws) muscle strength as an indicator of overall neuromuscular function according to the manufacturer's instructions. Data were reported in grams, normalized to mouse body weight. Each animal was tested three times, and the average value was recorded.

2.3 Transmission Electron Microscopy Analysis

The quadriceps femoris muscle (*vastus lateralis*) of the left hind limb of experimental mice (three samples per age group) were isolated and placed in ice-cold saline. Freshly harvested tissue fragments were stained with 2% osmium tetroxide (201030, Sigma-Aldrich, St. Louis, MO, USA), dehydrated through an ethanol series, infiltrated in Epon 812 (21045, Serva Electrophoresis, Heidelberg, Germany), and polymerized.

From the obtained Epon blocks, serial semi-thin sections (7 µm) were prepared on a Pyramitome LKB 11800 microtome (LKB AB, Bromma, Sweden). The longitudinal orientation of muscle fibers was controlled using an NU-2E microscope (Carl Zeiss, Germany, E25x Planachromat objective) using a Nikon digital camera (D5100, Nikon Corp., Tokyo, Japan) , and the identification of the mid-belly region of the quadriceps femoris was performed [24].

Histological sections were glued onto clean Epon blocks. The ultrathin sections (70–75 nm) were obtained from the blocks using a Leica EM UC6 ultramicrotome (Leica, Wetzlar, Germany), which were then counterstained with lead citrate (15326, Sigma-Aldrich, St. Louis, MO, USA) and uranyl acetate (22400, Electron Microscopy Services, Hatfield, PA, USA). Ultrastructural examination of the specimens was accomplished using a JEM-1400 electron microscope (JEOL, Tokyo, Japan) at the Electron Microscopy Facility at the Belozersky Institute of of Physico-Chemical Biology (MSU, Moscow, Russia).

The quantitative morphometric analysis of electron micrographs was executed using Fiji Image J2 software (National Institutes of Health, Bethesda, MD, USA) as described earlier [25]. Skeletal muscle tissue ultrastructure, including mitochondrial morphology, mitochondrial size (perimeter), and mean organelle number per unit area were analyzed in thirty non-overlapping fields of view in each age group. Mitochondria were considered intact if they had continuous outer and inner membranes, thin intermembrane spaces, and regular cristae membranes folded into a compact mitochondrial matrix. Organelles with enlarged intermembrane spaces and swollen cristae were defined as swollen. A total of approximately 100 mitochondrial cross-sectional profiles were collected per sample for each age group of animals.

2.4 Isolation and Analysis of Mitochondria from Mouse Skeletal Muscle

After the experimental mice were sacrificed, quadriceps muscle samples from both hind limbs were placed rapidly in ice-cold saline and processed for further differential centrifugation using a T25 digital Ultra Turrax disperser (IKA-Werke GmbH and Co. KG, Staufen, BW, Germany). The preparation of muscle mitochondria was fulfilled at 4 °C as reported previously [26,27]. The protein concentration of the final mitochondrial suspension was determined by the Bradford method using defatted BSA as a standard. Typically, the assay showed 30–40 mg protein/mL.

2.5 High-Resolution Respirometry

The respiration of freshly isolated mitochondria was analized using a high-resolution Oroboros Oxygraph-2k respirometer (Oroboros Instruments GmbH, Innsbruck, AT, Austria) in an incubation medium containing 2.5 mM potassium glutamate, 2.5 mM potassium malate, 100 mM KCl, 5 mM KH_2PO_4, 75 mM mannitol, 25 mM sucrose, 0.5 mM EGTA, and 10 mM HEPES/KOH (pH 7.4). The functional activity and oxidative phosphorylation efficiency of

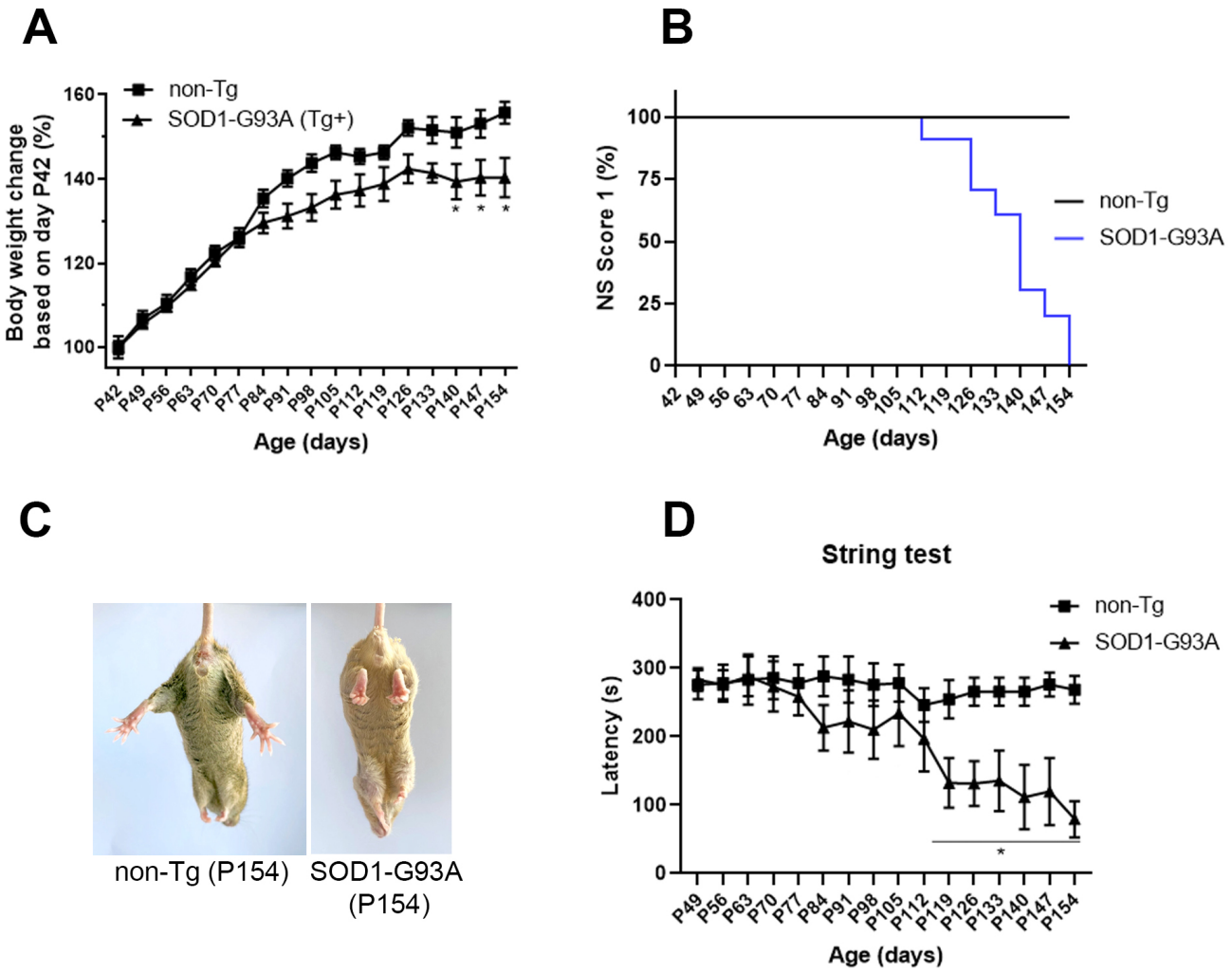

Fig. 1. Phenotypic observations and motor performance assessment of SOD1-G93A/low male mice ($n = 30$) compared with non-transgenic (non-Tg) littermates ($n = 34$). (A) Dynamic changes in body weight normalized to 100% the 42nd day of the postnatal period (P). (B) The neurological score (NS) data for experimental mice according to the neurological scoring system developed by the Institute for Advancement in ALS Therapy. (C) Tail suspension test used to assign neurological scores. The SOD1 transgenic mouse (right) exhibits prolonged hind limb clasping (onset of paresis) compared to the non-transgenic animal (left) at the end of the observation period (P154). The phenotype of the SOD1-G93A animal corresponds to NS 2. (D) Time course of the string test (paw grip endurance test) to assess general muscle function and coordination, with particular attention to limb grip strength. The time until the mouse falls (latency) was recorded in seconds after the animal grasped the wire with its forepaws. Values are mean ± SEM. *$p < 0.05$ significantly different from the non-Tg group, two-way analysis of variance with Bonferroni's post hoc test. Tg, transgenic; SOD1, copper-zinc superoxide dismutase; ALS, amyotrophic lateral sclerosis.

mouse skeletal muscle mitochondria (0.25 mg/mL) in different metabolic states were examined by calculating the rates of O_2 uptake (nmol/min/mg protein) in the presence of ADP at a concentration of 200 µM (phosphorylation or State 3 respiration), after its conversion into ATP (resting or State 4 respiration), and in the presence of 2,4-dinitrophenol at a concentration of 50 µM (uncoupled or State $3U_{DNP}$ respiration). Oxidative phosphorylation was assessed from the State 3/State 4 index, called the respiratory control ratio (RCR), and the time spent for the phosphorylation of 200 µM ADP (Tph) [28].

2.6 Assays of the Mitochondrial Calcium Retention Capacity Index and the Content of Lipoperoxidation Products

To assess the calcium retention capacity (CRC) index, mouse skeletal muscle mitochondria (0.2 mg protein/mL) were resuspended in an incubation medium containing 210 mM mannitol, 1 mM KH_2PO_4, 70 mM sucrose, 10 µM EGTA, and 10 mM HEPES-KOH buffer (pH 7.4.), and supplemented with the ion-sensitive indicator Arsenazo III (50 µM) (A92775, Sigma-Aldrich, St. Louis, MO, USA) [27]. The absorbance of the indicator was assessed using

a Spark 10M multimode microplate reader at 675 and 685 nm (Tecan, Männedorf, Switzerland). To induce the mPTP-related permeabilization of mitochondrial membranes, calcium chloride solution was added in 20 µM pulses until massive efflux of the ion from the matrix occurred. The final amount of added ion (nmol Ca^{2+}/mg mitochondrial protein) was used to calculate the CRC.

To determine the intensity of mitochondrial lipid peroxidation, the contents of thiobarbituric acid (TBA)-reactive substances in mouse skeletal muscle mitochondria from the age groups were estimated as described previously [29]. The transmission density was recorded on a Shimadzu Double Beam UV-2401PC UV-Vis spectrophotometer (Kyoto, Japan) at 650 and 532 nm *vs*. blank samples.

2.7 Statistical Data Processing

The results were processed using the GraphPadPrism 8.0.1 software (GraphPad Software, Inc., San Diego, CA, USA); data are given as the mean ± standard error of the mean (SEM). The Shapiro-Wilk test was applied to check the normality of data distribution. If the data were within the normal distribution, the statistical processing was performed using a two-way analysis of variance unless otherwise noted. The Bonferroni test was further applied as a *post hoc* analysis to compare the means of the dispersion complex. The statistical analysis of the electron microscopy data was based on the Mann-Whitney test. *p* values of less than 0.05 were considered significant.

3. Results

3.1 Phenotypic Observations and Assessment of Motor Abilities of Experimental Mice

To establish the pre-symptomatic and subsequent symptomatic stages of ALS progression in our cohort of male mice of the congenic line B6SJLTg(SOD1-G93A)dl1Gur/J, phenotypic analysis and assessment of motor activity of experimental animals were performed weekly in a preliminary series of experiments. The transgenic mouse model of ALS is characterized by ubiquitous expression of the low-copy-number *SOD1-G93A* transgene and develops pathological changes most similar to those seen in human fALS [20–22]. Littermates of the same sex who did not inherit the mutant gene were used as control (non-transgenic (non-Tg)) animals.

Fig. 1A shows a change in the body weight of experimental animals from the 42nd to the 154th day of the postnatal period (P). Non-Tg mice can be seen to show a stable increase in body weight, whereas SOD1-G93A animals stopped gaining weight at P126, after which a tendency towards a decrease in this indicator was observed compared to the maximum value. The difference in this integral index between SOD1 transgenic mice and control littermates became statistically significant at twenty weeks of age (P140).

By the end of the observation period (P154), all SOD1 transgenic animals showed signs of partial or complete paralysis of the hind limbs, consistent with abnormal neurological scores (NS >0) according to [23]. It is worth noting that non-transgenic animals demonstrated a normal phenotype (NS 0) from P42 to P154 (Fig. 1B). In the tail suspension test, SOD1-G93A mice at P154 spent 1 min or more with hind limbs clasped together, whereas age-matched non-transgenic controls exhibited no similar clasping phenotype during the observation time (Fig. 1C).

The string test (also known as the "paw grip endurance test" or "wire hanging test") was performed to assess the functional performance of skeletal muscle and overall coordination, with an increased focus on limb grip strength (Fig. 1D). SOD1 transgenic mice were found to have a 19% reduction in the latency to fall at twelve weeks of age (P84) compared to their peak value (P63). The difference in this parameter between the two study groups became significant at P84. At P154, the latency time was 268.4 ± 20.3 and 79.4 ± 26.5 s for the non-Tg and SOD1-G93A groups, respectively.

In addition, the grip strength test was used to determine motor ability and fatigue resistance as maximal muscle strength of hindlimbs (Fig. 2A), forelimbs (Fig. 2B), and combined hindlimbs and forelimbs (Fig. 2C) of experimental mice. At eight weeks of age (P56), the normalized grip strength (g (force)/g (weight)) displayed by mice using all four limbs did not differ between the two groups. Beginning at P84, SOD1-G93A mice showed a decline in maximal muscle strength of hindlimbs and combined hindlimbs and forelimbs, which became more pronounced as the pathology progressed. Regarding forelimb grip strength, a statistically significant difference between the two groups was found at P91.

Thus, detailed behavioral monitoring revealed three specific phenotypes (age groups): postnatal (P) days 56 (P56), 84 (P84) and 156 (P154), considered as the pre-symptomatic, early symptomatic (or late pre-symptomatic) and symptomatic (advanced) stages of disease progression and severity in SOD1-G93A/low mice, respectively. Animals from these three age groups, 10 mice each, were used to study the successive stages of ALS development further.

3.2 Stage-Dependent Alterations in Mitochondrial Ultrastructure in the Quadriceps Femoris Muscle of SOD1-G93A/Low Mice

Skeletal muscle fibers heavily rely on mitochondria as a metabolic hub and an important contributor to energy production to maintain their high activity [11]. Therefore, we further studied the changes in the ultrastructure of mitochondria in muscle fibers of identical tissue samples (quadriceps femoris) in non-transgenic and SOD1-G93A/low animals as they aged and the disease progressed.

Figs. 3,4,5 show typical transmission electron microscopy (TEM) micrographs of longitudinal sections of the quadriceps femoris from mice of three age groups: P56, P84, and P154. Ultrastructural examination showed that

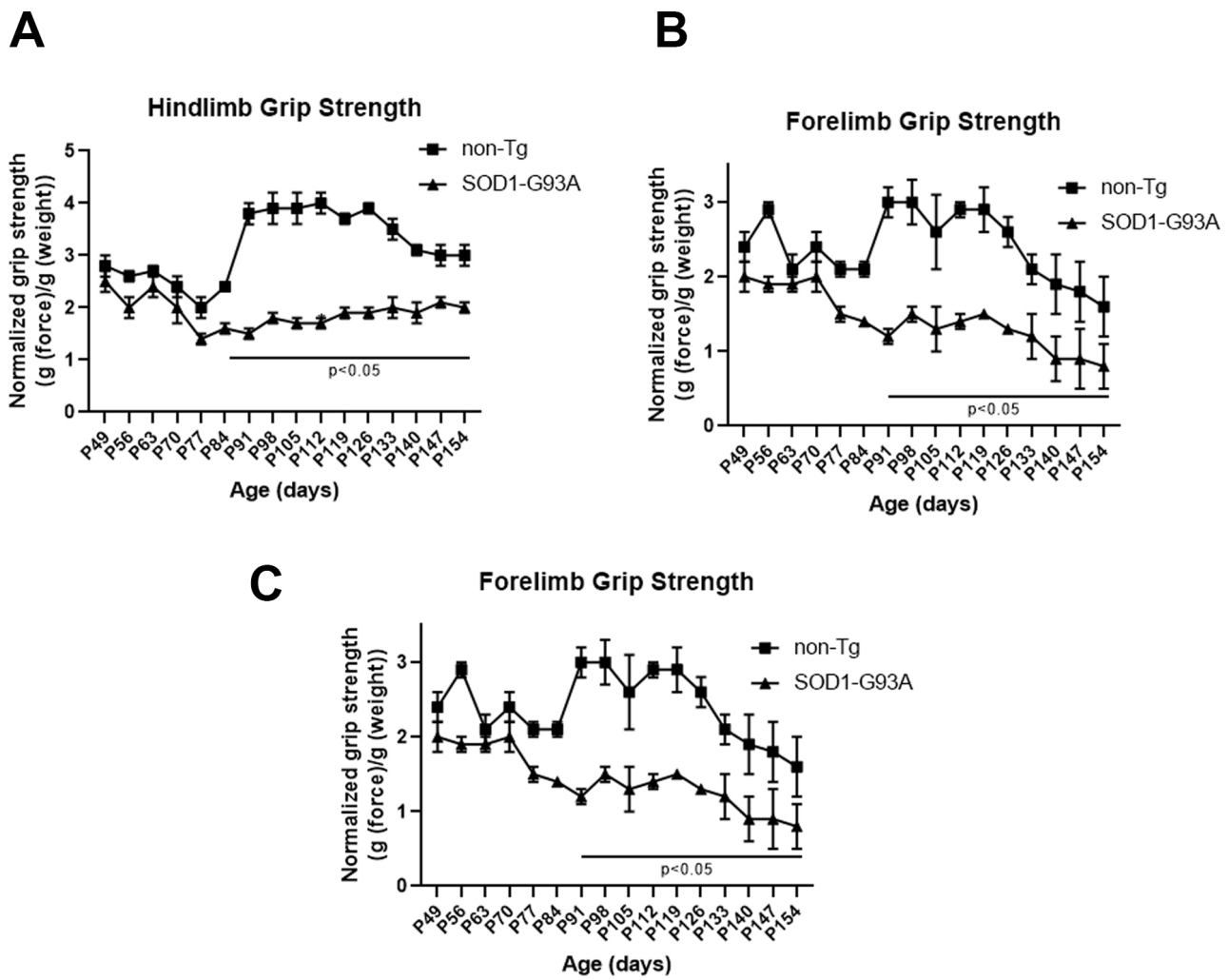

Fig. 2. Dynamics of the functional performance of skeletal muscles as maximal muscle strength of hindlimbs (A), forelimbs (B), and combined hindlimbs and forelimbs (C) in mice of experimental groups, as assessed by the grip strength test. Values are mean ± SEM (n = 30–34). $p < 0.05$, two-way analysis of variance with Bonferroni's post hoc test.

at the pre-symptomatic stage (P56), the contractile apparatus (sarcomeres and myofibrils) and mitochondria in SOD1 transgenic animals had a classical architecture and did not differ from the control non-transgenic group (Fig. 3; **Supplementary Fig. 1**). Of particular interest was the subsarcolemmal region, positioned at the periphery of the myofiber, directly beneath the sarcolemma. In this fiber region, mitochondria were clustered and had spherical or elongated regular shapes. Mitochondria had predominantly dark condensed matrix and tightly packed cristae, indicating a functionally active (high-energy) metabolic state.

Mosaic destructive alterations in subsarcolemmal mitochondria in the fibers of the quadriceps femoris muscle were detected in SOD1-G93A/low animals at the early symptomatic stage of ALS progression (age group P84) (Fig. 4; **Supplementary Fig. 2**). Some organelles were swollen, had fragmented crista membranes and areas of sharp enlightenment of the mitochondrial matrix. These findings are in line with the results of some studies showing accumulation of mutant protein aggregates into mitochondria, leading to disruption of mitochondrial membrane integrity and mitochondria-associated endoplasmic reticulum membranes [17,18].

At the age of 154 days, the structure of the fibers of the quadriceps femoris from non-transgenic animals did not change, and mitochondria in the subsarcolemmal region had a typical morphology and disposition (Fig. 5A,B). In this group, no abnormalities in the internal organization of the cristae or perturbations of the mitochondrial membranes were observed. In contrast, SOD1-G93A/low mice at P154 exhibited pronounced pathological changes in mitochondria, sarcoplasmic reticulum, and sarcomeres (Fig. 5C,D). This group showed a disruption of the regular organization of the sarcomere, along with a reduction in the width of this basic contractile unit, an expansion of the sarcoplasmic regions between myofibrils, and fiber splitting. In these muscle fibers, the Z-lines of adjacent myofibrils tended to lose contact with each other and became curved. Under-

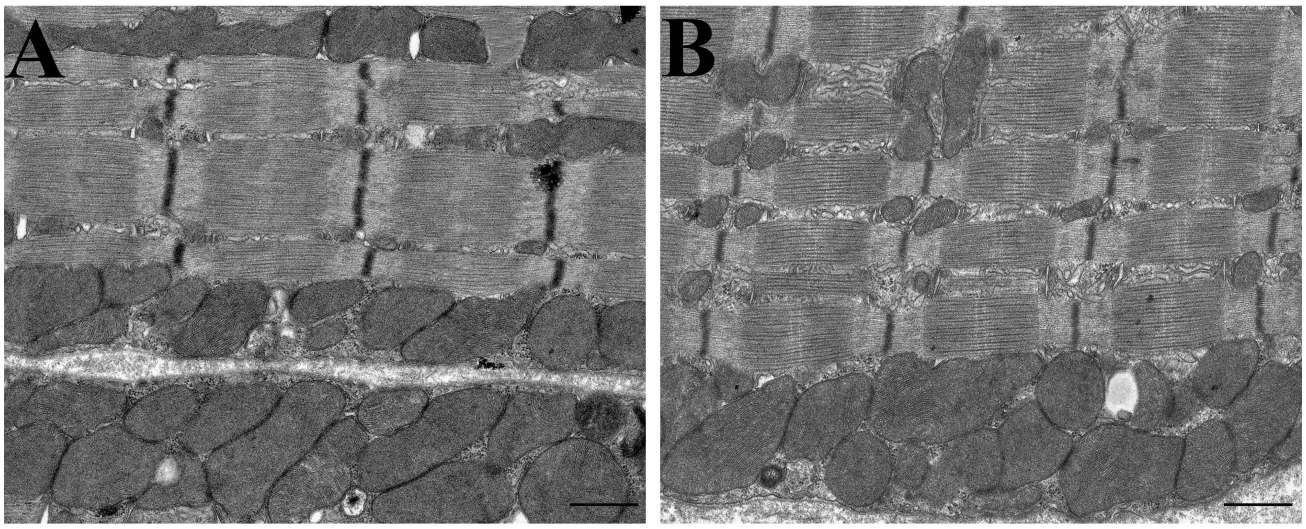

Fig. 3. Representative TEM micrographs of mitochondria of the subsarcolemmal fiber region of the quadriceps femoris from non-transgenic (A) and SOD1-G93A (B) male mice at P56, established as the pre-symptomatic stage of ALS progression. High magnification images (×5000). In both groups, the mitochondria had a typical morphology; no abnormalities in crista membranes were observed. The scale bar is 1 µm. TEM, Transmission electron microscopy.

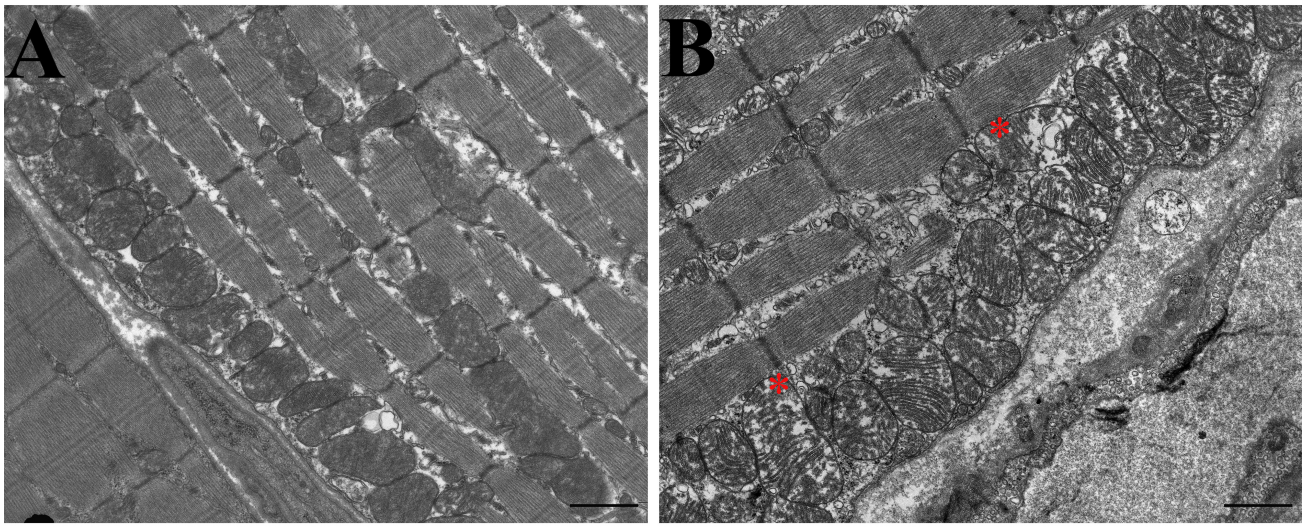

Fig. 4. Representative TEM micrographs of subsarcolemmal mitochondria of the quadriceps femoris from non-transgenic (A) and SOD1-G93A (B) male mice at P84, established as the early symptomatic stage of ALS progression. In muscle fibers from SOD1 transgenic animals, peripheral (subsarcolemmal) mitochondrial clusters are larger and contain damaged (vacuolated) organelles. Red asterisks indicate vacuolated mitochondria. High magnification images (×5000). The scale bar is 1 µm.

neath the sarcolemma, swollen mitochondria with enlarged intermembrane spaces and deformed crista lumens predominated; ruptures were observed in the outer membrane of many mitochondria. Also worth noting is the appearance of giant interfibrillar mitochondria, which are grouped in longitudinal rows between the myofibrils (**Supplementary Fig. 3**). These mitochondria are damaged (vacuolated) and have an edematous matrix with disrupted or missing outer and cristae membranes. It is known that the morphology and disposition of mitochondria in muscle cells may influence myofilament interactions and sarcomere structure. Interestingly, similar abnormalities in mitochondria and contractile apparatus organization have been reported in skeletal muscle biopsies from ALS-affected individuals [30].

Quantitative morphometric analysis was performed to identify the alterations in the number and mean size of mitochondria, as well as the length and width of the sarcomere in the investigated animal groups (Fig. 6). Analysis of the morphometric characteristics in the SOD1-G93A mouse group at P154 revealed a decrease in the number of subsarcolemmal mitochondria normalized to the area of the analyzed micrographs. In addition, a compensatory increase

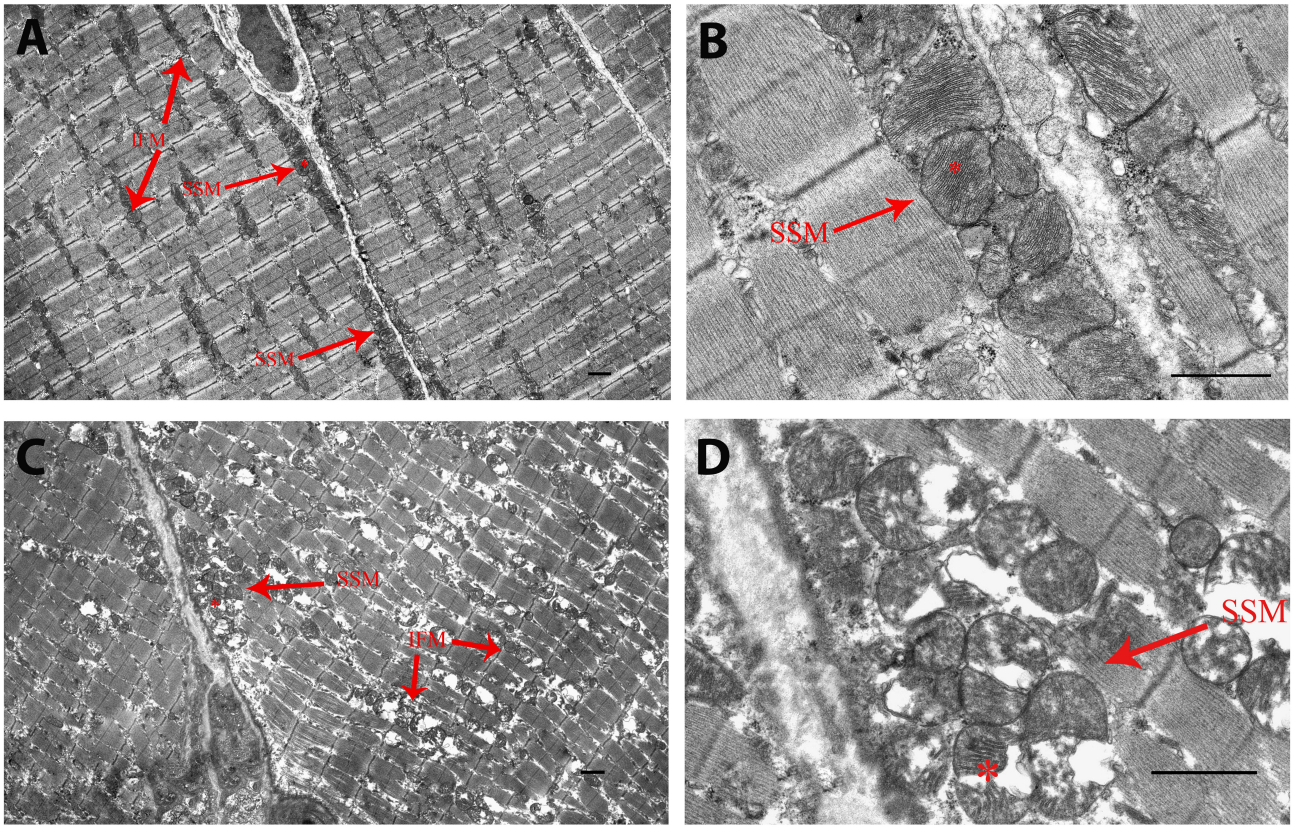

Fig. 5. Representative TEM micrographs of longitudinal sections of the quadriceps femoris from non-transgenic (A,B) and SOD1-G93A transgenic (C,D) male mice at P154 (late symptomatic stage) at low (×1500) and high (× 5000) magnification. Red arrows point to the interfibrillar subpopulation of mitochondria (IFM) and the subsarcolemmal subpopulation of mitochondria (SSM). The same organelles are indicated by an asterisk in the low- and high-magnification micrographs. In the SOD1-G93A group, the mitochondria demonstrated vacuolization and abnormal or missing internal cristae due to their local lysis (shown by arrows). The scale bar is 1 μm.

in this parameter was observed in SOD1-G93A animals at P84. Along with this, the mean size of subsarcolemmal mitochondria in SOD1 transgenic mice at P84 and P154 increased compared to that in the control group.

The results confirm the pronounced swollen state of skeletal muscle mitochondria in these two age groups of transgenic animals.

It should be pointed out that the sarcomere length did not change significantly between the experimental groups. Notably, the sarcomere width in the quadriceps femoris muscle of SOD1-G93A transgenic mice decreased at P154, which may indirectly indicate disorganization of the contractile apparatus (myofibrils).

3.3 Functional Assessment of Mitochondria in the Quadriceps Femoris of SOD1-G93A/low Animals of the Age Groups P56, P84, and P154

The structure of mitochondria is inextricably linked with their multiple functions in skeletal muscle fibers. In the next part of the study, we investigated the main functional parameters of these organelles isolated from the quadriceps femoris of the groups of animals under study.

One of the key criteria for skeletal muscle mitochondrial functionality is the efficiency of oxidative phosphorylation, conventionally analyzed using high-resolution respirometry (Oroboros Oxygraph-2k). Study has shown that the the first enzyme complex NADH: ubiquinone oxidoreductase of the mitochondrial respiratory chain (complex I) is the least resistant to damage in muscle pathologies [11], so we measured the respiration rates of mitochondria in three metabolic states (States 3, 4, and $3U_{DNP}$) using the NAD-related substrates malate and glutamate (Table 1). Typical Oxygraph-2k records for respiration of mouse skeletal muscle mitochondria are presented in **Supplementary Fig. 4**.

Skeletal muscle mitochondria from SOD1-G93A animals at P154 (symptomatic stage) were found to demonstrate a decrease in the rates of ADP-stimulated (phosphorylating) (V_3) and uncoupled (V_{3UDNP}) respiration. Moreover, a decline in the respiration control ratio (State 3/State 4, RCR) and an increase in the time of ADP phosphorylation (Tph), as compared to the control values, were revealed. Taken together, this suggests a decrease in the maximum efficiency of the mitochondrial electron trans-

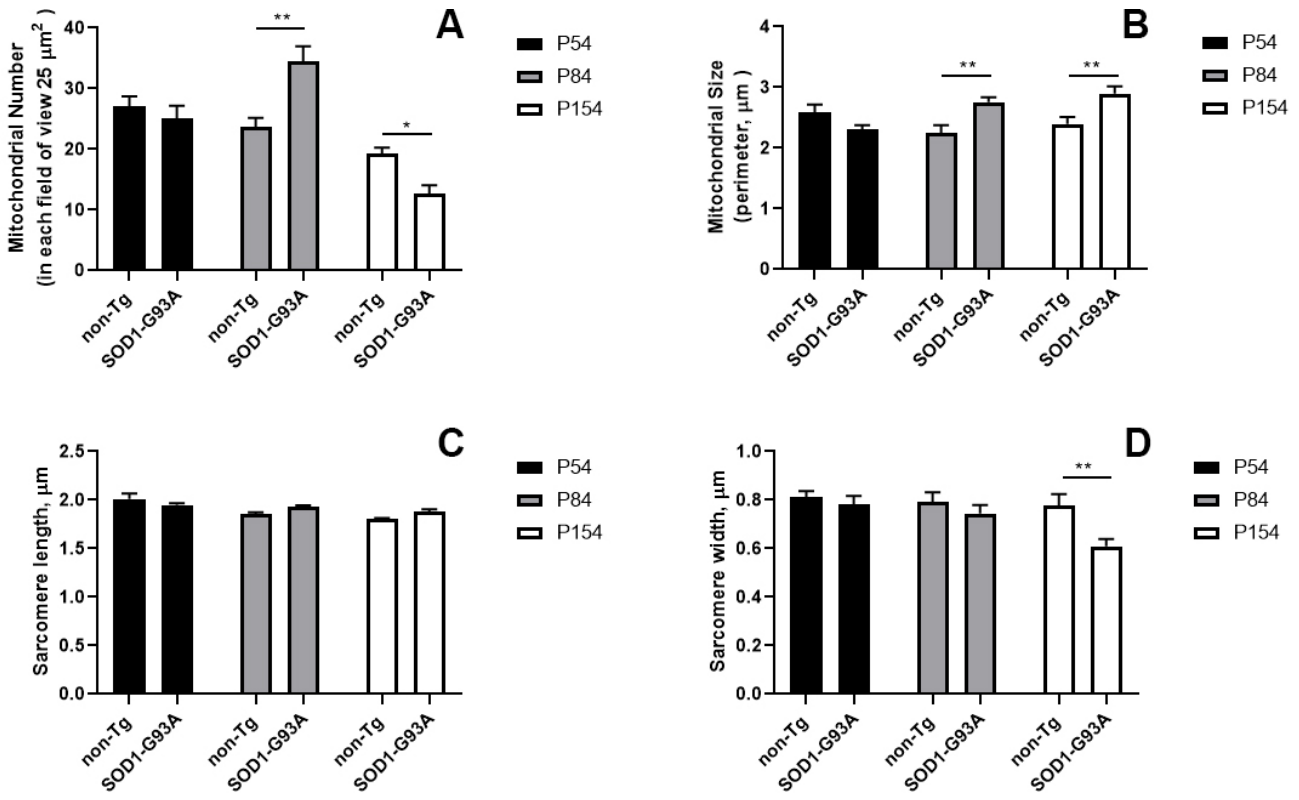

Fig. 6. Morphometric analysis of subsarcolemmal mitochondria and sarcomeres from skeletal muscle (quadriceps femoris) of male non-transgenic (non-Tg) and SOD1-G93A mice from three age groups: P56, P84, and P154. Histograms summarizing (A) the number of the organelles per unit area, (B) mitochondrial size (perimeter), (C) the length of the sarcomere (μm), and (D) the width of the sarcomere (μm) in the animal groups. Analyses were performed on at least three animal tissue samples (thirty non-overlapping fields of view) per group. Values are mean values ± SEM. * $p < 0.05$, ** $p < 0.01$, compared with the non-Tg group.

port chain for ATP synthesis. It should be pointed out that the respiration rates of mitochondria from the quadriceps femoris of SOD1 transgenic animals at P56 and P84 did not significantly differ from those in the age-matched non-Tg groups.

As is known, abnormal accumulation of calcium ions in mitochondria can lead to organelle damage via the permeability transition pore (PTP) opening and ROS overproduction, ultimately leading to the activation of cell death processes [31]. Given the important role of mitochondria in maintaining calcium and redox homeostasis, we determined the calcium retention capacity index to predict susceptibility to the PTP formation and the content of lipid peroxidation products (malondialdehyde and other minor aldehydes), assessed by the 2-thiobarbituric acid (TBA) method (Fig. 7).

One can see that SOD1-G93A mice at P154 demonstrated a lower capacity of skeletal muscle mitochondria to retain calcium cations and increased levels of mitochondrial TBA-reactive substances compared with those in the control non-Tg group. The latter may indicate increased oxidative injury to muscle mitochondria from SOD1-G93A animals in disease progression.

4. Discussion

ALS is associated with an age-dependent decline in the mass and functional performance of the body's skeletal muscles; the key pathological changes in affected muscle fibers remain poorly understood [2]. Accumulating evidence suggests that skeletal myocyte mitochondria are crucial targets in ALS pathogenesis, and their dysfunction and associated oxidative stress affect the progression of ALS [32,33]. Despite some progress in understanding the genetic basis of the pathology, in particular the role of *SOD1* mutations [4,34], there is still no unified hypothesis that combines mitochondria-related mechanisms with other intracellular events implicated in ALS, taking into account their time course and localization [35,36]. The latter may significantly complicate the development of effective approaches to target molecular pathways through combined therapy for ALS at its different stages.

In this study, we analyzed the dynamics of structural and functional rearrangements in mitochondria from the quadriceps femoris muscle of SOD1-G93A/low transgenic animals and related these rearrangements with motor impairment and skeletal muscle weakness at three time points corresponding to pre-symptomatic (P56), early symptomatic (P84), and late symptomatic (advanced) stages

Table 1. Indices of respiration and oxidative phosphorylation of mouse skeletal muscle mitochondria from the age groups under study.

Stage	Group	V respiration, nmol O_2 × min^{-1} × mg^{-1} protein			RCR	T_{ph}
		State 3	State 4	State $3U_{DNP}$		
P56	Non-Tg	183.3 ± 10.4	40.3 ± 1.4	325.3 ± 6.4	4.55 ± 0.22	32.5 ± 2.0
	SOD1-G93A	180.9 ± 5.3	43.5 ± 1.5	300.1 ± 20.8	4.16 ± 0.19	34.0 ± 4.1
P84	Non-Tg	169.3 ± 4.2	37.8 ± 1.4	252.3 ± 8.2	4.73 ± 0.34	43.3 ± 3.4
	SOD1-G93A	165.9 ± 5.3	36.5 ± 3.0	240.4 ± 17.6	4.64 ± 0.31	43.4 ± 2.9
P154	Non-Tg	144.6 ± 4.2	32.0 ± 1.2	230.9 ± 10.4	4.57 ± 0.20	50.3 ± 3.0
	SOD1-G93A	127.8 ± 2.8 **	31.0 ± 0.8	177.7 ± 10.0 **	4.08 ± 0.10 *	67.2 ± 5.9 *

The experimental conditions are described in detail in the Materials and Methods section. Values are means ± SEM (n = 6). * $p < 0.05$, ** $p < 0.01$, compared with the non-Tg group, two-way analysis of variance with Bonferroni's post hoc test. RCR, respiratory control ratio; SOD1, copper-zinc superoxide dismutase; Non-Tg, non-transgenic.

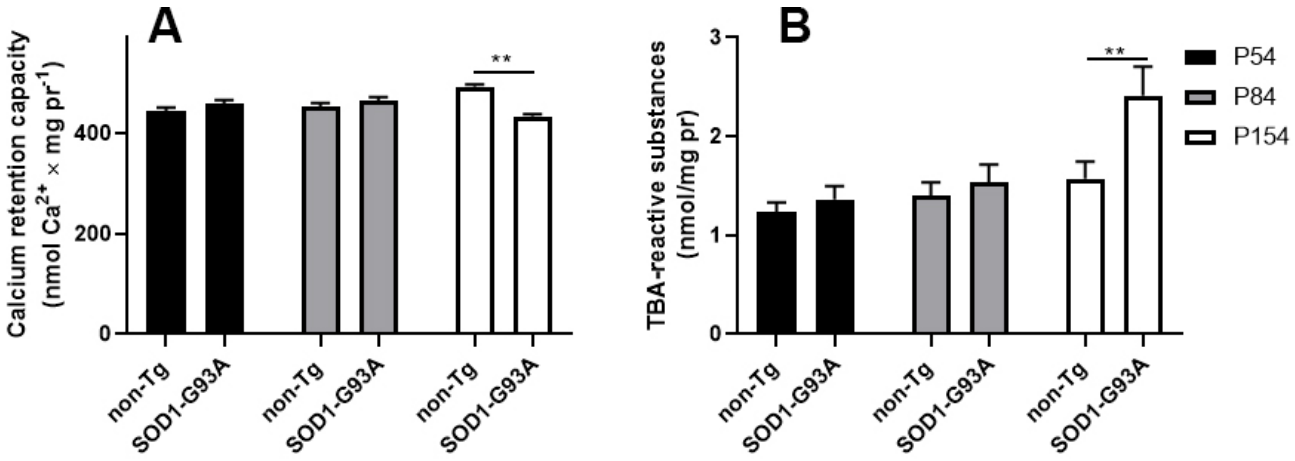

Fig. 7. Functional analysis of mitochondria from the quadriceps femoris of non-transgenic (non-Tg) and SOD1-G93A male mice from three age groups, established as pre-symptomatic (P54), early symptomatic (P84), and advanced symptomatic (P154) stages. (A) Calcium retention capacity, an index of susceptibility to the mPTP opening and (B) the level of 2-thiobarbituric acid (TBA)-reactive substances (byproducts of lipid peroxidation) in skeletal muscle mitochondria from the age groups under study. Values are mean ± SEM (n = 5–6). ** $p < 0.01$, compared with the non-Tg group, two-way analysis of variance with Bonferroni's post hoc test.

(P154) of ALS. This mouse line is the most widely recognized transgenic model for studying fALS and is well characterized genotypically, with accumulation of the ALS-causing mutant SOD1-G93A in skeletal muscle tissue shown to be associated with muscle degeneration [37]. The data obtained suggest that in the SOD1-G93A mouse model, mitochondrial abnormalities and energy metabolism disorders at the level of skeletal muscle fibers appear with the onset of motor symptoms at P84 and progress with the animal's age.

To establish the specific time points in the progression of the disease, age-dependent changes in motor functions and neurological status of SOD1-G93A male mice, as compared to non-transgenic animals, were determined weekly using two behavioral tests: the paw grip endurance test and the grip strength test. Previous studies have identified pathological events in muscle function in the mutant SOD1 mouse models; however, subtle phenotypic differences between the genotypes have been observed [20–22, 38]. It should be noted that the Tg(SOD1G93A)dl1/GurJ mouse substrain (referred to as SOD1-G93A/low mice) has a lower (20–25) copy number of human *SOD1* cDNA compared with other mutant SOD1 mouse models [39]. Moreover, study in SOD1-G93A mouse models and ALS-affected individuals suggests that males have more pronounced changes in some disease-related molecular pathways compared to females [40]. In our animal cohorts, 12-week-old (P84) SOD1 transgenic male mice demonstrated a significant decrease in the tightrope hang time compared to their maximal values at P56 and those of non-transgenic littermates, and then showed a progressive decline in the test results until the final week of observation (P154). Furthermore, normalized grip strength in SOD1-G93A mice began to decline at 12 weeks of age (P84), and by P154 it

was reduced 2-fold compared to non-transgenic mice, as assessed by the grip strength test. In parallel, it was found that SOD1-G93A mice began to lose body weight at the age of 16 weeks (P112), and by the end of the experiment (P154) had a significant difference in weight gain as compared with control animals.

It is worth mentioning that progressive muscle weakness and functional disorders of skeletal muscle fibers have been reported in many transgenic mouse models and patients with sALS and fALS [14,17], but muscle abnormalities were historically interpreted as secondary to motor neuron disease [6,9]. Recent studies have shown that transgenic mice expressing the pathogenic G93A variant of the *SOD1* gene only in skeletal muscle, but not specifically in motor neurons, develop a fatal ALS-like phenotype, suggesting that skeletal muscle is a crucial target tissue in disease progression and severity [31,32]. Few studies have systematically examined the pathogenesis of ALS in the context of the development of mitochondrial damage in the peripheral components of the neuromuscular system, including skeletal muscle [37–41].

Our study identified the dynamics of ultrastructural alterations in myocytes and mitochondria in the quadriceps femoris of SOD1 animals at P56, P84, and P154 – the stages that had been established as pre-symptomatic, early and late symptomatic when monitoring the behavioral phenotype in the study cohort of animals. Ultrastructural examination showed early mosaic destructive changes in the mitochondria located underneath the sarcolemma of quadriceps femoris fibers from SOD1-G93A/low mice at P84. At this stage, individual swollen mitochondria had a matrix with low electron density and fragmented cristae. These findings could represent early markers for the onset of the pathology.

At P154, ALS-related abnormalities in subsarcolemmal mitochondria include extensive swelling of the matrix, leading to crista depletion and outer membrane rupture. In addition, we observed giant intrafibrillar mitochondria, which are grouped in longitudinal rows between the myofibrils. These mitochondria are vacuolated and have an edematous matrix with disrupted or missing outer and cristae membranes. The appearance of these mitochondria within muscle cells can disrupt the structure and function of the basic contractile unit of muscle, the sarcomere. Furthermore, pathological morphological features of muscle disease were identified, including Z-line curvature, sarcomere disorganization, an expansion of the sarcoplasmic regions between myofibrils, and fiber splitting in the quadriceps femoris from SOD1-G93A mice at the late symptomatic stages of ALS progression.

Morphometric analysis revealed an increase in the mean size (perimeter) of subsarcolemmal mitochondria in the quadriceps femoris of SOD1-G93A mice at the early and late symptomatic stages of the pathology, indicating a swollen state of the organelles. It is noteworthy that at the early stage (P84), an increase in the number of muscle mitochondria under the sarcolemma was observed, and then as motor symptoms intensified at P154, their count decreased. One can suggest that the increase in the number of mitochondria at the early symptomatic stage indicates the activation of compensatory mechanisms to maintain mitochondrial homeostasis in skeletal muscle. Several studies have identified abnormal activation of AMP-activated protein kinase (AMPK), a key sensor of cellular energy status, in various ALS models and patients, which may be accompanied by increased mitochondrial biogenesis, imbalance in their turnover, and contribute to ALS pathogenesis [42,43]. Furthermore, the P154 transgenic group demonstrated a decrease in the mitochondrial number, suggesting the prevalence of maladaptive processes, including those leading to mitochondria-mediated cell death in affected muscle fibers. Since the subsarcolemmal mitochondrial subpopulation is responsible for membrane-related processes [11,13], this may contribute to a bioenergetic crisis in substrate transport, ion exchange, and signal transduction – steps that are clearly relevant to skeletal muscle function and are impaired in ALS [1,14]. Several studies using *in vitro* and *in vivo* models for ALS have demonstrated that mutant forms of the SOD1 protein can accumulate inside mitochondria, mainly in the intramembrane mitochondrial space, and thus cause disturbances in their ultrastructure [18,37,38]. This may lead to the formation of giant mitochondria and the appearance of mitochondrial paracrystalline inclusions, as shown in skeletal muscle from ALS patients [30]. Unfortunately, we did not detect these inclusions in the mitochondria of the quadriceps femoris from of SOD1-G93A mice. Other pathological structural alterations, including mitochondrial vacuolization and the appearance of giant organelles between myofibrils, were similar.

Pathological accumulation of ALS-associated mutant proteins inside mitochondria could impair the functional activity of mitochondria and cells [41]. This study found that, as the SOD1-G93A animals aged, the efficiency of the mitochondrial respiratory chain gradually declined, which led to a decrease in the rate of State 3 (ADP-stimulated) and State $3U_{DNP}$ (uncoupled) respiration driven by the NAD-dependent substrates malate and glutamate. It is known that disturbances in the functioning of the respiratory chain complex-I activity can be accompanied by a deficiency of ATP and excessive production of ROS by mitochondria [44,45], which can ultimately result in a disruption of muscle contraction. These findings are consistent with emerging data indicating a bioenergetic deficit in ALS, with one-half of patients demonstrating hypermetabolic energy expenditure at rest [46,47]. Interestingly, littermate controls did not show a similar trend in bioenergetic parameters of skeletal muscle mitochondria with age.

Some studies have shown that mitochondrial bioenergetics in ALS-affected cells can be regulated by PINK1/Parkin-dependent and -independent mitophagy pathways [48,49] and the transcription regulator PGC-1α

(peroxisome proliferator-activated receptor-1-alpha-coactivator) [50], as well as mitochondrial fission and fusion mediated mainly by dynamin-related protein 1 and mitofusin 2, respectively [37,51]. In addition, the expression of the *Nfe2l2* gene, encoding the transcription factor NRF2 that regulates the expression of more than a hundred cytoprotective genes, including those of antioxidant defense, has been found to undergo dramatic changes in ALS [52]. NRF2 has been shown to play a key role in mitochondrial quality control and regulation of key mitochondrial functions, including ATP synthesis, ROS production, and calcium ion transport [51,52]. Notably, levels of the alpha subunit of AMPK, a key regulator of cellular energy and catabolism, are also altered in various ALS models [53,54].

The generation of ROS in mitochondria depends on their metabolic state and the membrane potential [55]. Our experiments showed a sharp increase in the level of the arachidonate by-product malondialdehyde (and other minor aldehydes that react with thiobarbituric acid) in skeletal muscle mitochondria of SOD1-G93A mice at P154 compared to that in control age-matched animals, suggesting increased lipid peroxidation and oxidative damage to the organelles.

In addition to their classical roles as the sites of energy production and the formation of harmful ROS, mitochondria are also known to be involved in other skeletal myocyte functions that are impaired in ALS, including the maintenance of calcium ion homeostasis [11,31]. Mitochondrial calcium uptake, sequestration, and release play pivotal roles in orchestrating cellular ion homeostasis and responses, while a dyshomeostasis of calcium can result in mitochondrial injury through the calcium-dependent permeability transition pore (PTP) opening [31]. The formation of the PTP in mitochondria is associated with a sharp increase in ROS production, which leads to damage to key cellular components, including membrane lipids, and triggers cell death in ALS [55,56]. Notably, skeletal muscle mitochondria of transgenic mice at P154 showed a decreased ability to retain calcium ions (referred to as the calcium retention capacity index), indicating an increased susceptibility of the organelle to the mitochondrial permeability transition pore opening. The mPTP represents itself as a highly-reproducible, calcium-dependent increase in permeability of the inner membrane to ions and proapoptotic proteins (cytochrome *c*, apoptosis-induced factor, etc.) [31,56]. Study has shown that transient overexpression of mutated *SOD1* in skeletal muscle of wild type mice could promote an increased expression of cyclophilin D, the main regulatory component of the mPTP [33]. Recent findings have also revealed that treatment with highly selective blockers of the mPTP can delay the onset of motor deficit in transgenic ALS mice [57], indicating an important role of this phenomenon in the progression of mitochondrial dysfunction and muscle atrophy.

Taken together, the data obtained suggest that abnormalities in the morphology and distribution of the mitochondria, associated with their complex dysfunction and oxidative damage in the skeletal muscle of SOD1-G93A mice, underlie the occurrence of muscle weakness and contribute to the progression of ALS with age. It is known that in muscular dystrophic diseases, the subsarcomeric regions of muscles are mainly affected. It can be assumed that the loss of grip strength in SOD1-G93A mice is closely related to subsarcomeric alterations, since the anchoring of actin and other contractile proteins to this area of the myofibers is what allows the muscle force to be exerted. At the late stage, irreversible structural and functional abnormalities in mitochondria both beneath the sarcolemma and between myofibrils may ultimately lead to tissue damage and muscle fiber death. It can be concluded that the dynamics of the mitochondrial defects in skeletal muscle in SOD1 mouse model may further form the basis for the development of methods for early diagnosis and therapy or symptomatic correction of motor symptoms in ALS. It should be noted that several studies have shown that modulation of skeletal muscle metabolic pathways in SOD1-G93A mice reduces motor neuron death [58].

5. Conclusions

Using the SOD1-G93A/low transgenic mouse model, we demonstrated in this study stage-dependent changes in skeletal muscle mitochondrial ultrastructure and functions attributable to defective oxidative phosphorylation, impaired calcium homeostasis, and oxidative damage. Mosaic destructive alterations in subsarcolemmal mitochondria in quadriceps femoris fibers could precede the appearance of motor deficits and contribute to the progression of ALS with age. Thus, targeting these mechanisms of mitochondrial dysfunction in skeletal muscle, which represents the largest tissue mass in the body, appears to be a promising avenue for the development of combination therapies in the future. Our results also confirm that the SOD1-G93A/low mouse model is a suitable platform for studying long-term motor symptoms and associated mitochondrial alterations. However, changes in the main functional parameters of skeletal tissue mitochondria do not precede early impairments in muscle strength and functional activity *in vivo*. Further studies are required to explore the underlying effect of *SOD1* mutations on skeletal muscle mitochondria through modulation of the turnover of affected mitochondria and the redox imbalance-related mechanisms involved.

Abbreviations

ALS, amyotrophic lateral sclerosis; mPTP, mitochondrial permeability transition pore; SOD1, superoxide dismutase [Cu-Zn]; TBA, thiobarbituric acid.

Availability of Data and Materials

The datasets generated during the study are not publicly available as they will be used in the next mechanism research, but are available from the corresponding author on reasonable request.

Author Contributions

NVB designed the research study. NVB, AII, MVD, IBM, and KNB performed the research and analyzed the data. AII, MVD, and KNB conducted weekly behavioral phenotyping, collected samples, isolated mitochondria, performed their functional analysis, and interpreted the data. NVB and IBM performed TEM analysis. NVB and KNB wrote the manuscript. All authors contributed to editorial changes in the manuscript. All authors read and approved the final manuscript. All authors contributed sufficiently to the work and agreed to be accountable for all aspects of the study.

Ethics Approval and Consent to Participate

All animal procedures were conducted in strict compliance with the European Convention for the Protection of Vertebrates used for experimental and other purposes (Strasbourg, 1986). The study on laboratory animals was approved by the Institute of Theoretical and Experimental Biophysics RAS Ethics Committee (Protocol No. 02/2023 of 08 February 2023).

Acknowledgment

The JEM-1400 electron microscope (JEOL, Tokyo, Japan) at the Superresolution Microscopy and Spectroscopy core facility at the Belozersky Institute of Physicochemical Biology (Moscow, Russia) was used in this work. The authors are grateful to Viktor Selivanov for his help in proofreading the English language of the manuscript.

Funding

The work was supported by the Russian Science Foundation, grant No. 23-25-00286 awarded to N.V.B.

Conflict of Interest

The authors declare no conflict of interest. Mikhail V. Dubinin is serving as one of the Guest editors of this journal. We declare that Mikhail V. Dubinin had no involvement in the peer review of this article and has no access to information regarding its peer review. Full responsibility for the editorial process for this article was delegated to Gianluca Paventi.

Supplementary Material

Supplementary material associated with this article can be found, in the online version, at https://doi.org/10.31083/FBL28260.

References

[1] Al-Khayri JM, Ravindran M, Banadka A, Vandana CD, Priya K, Nagella P, *et al*. Amyotrophic Lateral Sclerosis: Insights and New Prospects in Disease Pathophysiology, Biomarkers and Therapies. Pharmaceuticals (Basel, Switzerland). 2024; 17: 1391. https://doi.org/10.3390/ph17101391.

[2] Duranti E, Villa C. From Brain to Muscle: The Role of Muscle Tissue in Neurodegenerative Disorders. Biology. 2024; 13: 719. https://doi.org/10.3390/biology13090719.

[3] Sharma R, Khan Z, Mehan S, Das Gupta G, Narula AS. Unraveling the multifaceted insights into amyotrophic lateral sclerosis: Genetic underpinnings, pathogenesis, and therapeutic horizons. Mutation Research. Reviews in Mutation Research. 2024; 794: 108518. https://doi.org/10.1016/j.mrrev.2024.108518.

[4] Müller K, Oh KW, Nordin A, Panthi S, Kim SH, Nordin F, *et al*. De novo mutations in *SOD1* are a cause of ALS. Journal of Neurology, Neurosurgery, and Psychiatry. 2022; 93: 201–206. https://doi.org/10.1136/jnnp-2021-327520.

[5] Wolfson C, Gauvin DE, Ishola F, Oskoui M. Global Prevalence and Incidence of Amyotrophic Lateral Sclerosis: A Systematic Review. Neurology. 2023; 101: e613–e623. https://doi.org/10.1212/WNL.0000000000207474.

[6] Eisen A. The Dying Forward Hypothesis of ALS: Tracing Its History. Brain Sciences. 2021; 11: 300. https://doi.org/10.3390/brainsci11030300.

[7] Scaricamazza S, Salvatori I, Ferri A, Valle C. Skeletal Muscle in ALS: An Unappreciated Therapeutic Opportunity? Cells. 2021; 10: 525. https://doi.org/10.3390/cells10030525.

[8] Quessada C, Bouscary A, René F, Valle C, Ferri A, Ngo ST, *et al*. Skeletal Muscle Metabolism: Origin or Prognostic Factor for Amyotrophic Lateral Sclerosis (ALS) Development? Cells. 2021; 10: 1449. https://doi.org/10.3390/cells10061449.

[9] Sbarigia C, Rome S, Dini L, Tacconi S. New perspectives of the role of skeletal muscle derived extracellular vesicles in the pathogenesis of amyotrophic lateral sclerosis: the 'dying back' hypothesis. Journal of Extracellular Biology. 2024; 3: e70019. https://doi.org/10.1002/jex2.70019.

[10] Katare PB, Dalmao-Fernandez A, Mengeste AM, Hamarsland H, Ellefsen S, Bakke HG, *et al*. Energy metabolism in skeletal muscle cells from donors with different body mass index. Frontiers in Physiology. 2022; 13: 982842. https://doi.org/10.3389/fphys.2022.982842.

[11] Dong H, Tsai SY. Mitochondrial Properties in Skeletal Muscle Fiber. Cells. 2023; 12: 2183. https://doi.org/10.3390/cells12172183.

[12] Hood DA. Invited Review: contractile activity-induced mitochondrial biogenesis in skeletal muscle. Journal of Applied Physiology (Bethesda, Md.: 1985). 2001; 90: 1137–1157. https://doi.org/10.1152/jappl.2001.90.3.1137.

[13] Ritov VB, Menshikova EV, He J, Ferrell RE, Goodpaster BH, Kelley DE. Deficiency of subsarcolemmal mitochondria in obesity and type 2 diabetes. Diabetes. 2005; 54: 8–14. https://doi.org/10.2337/diabetes.54.1.8.

[14] Kubat GB, Picone P. Skeletal muscle dysfunction in amyotrophic lateral sclerosis: a mitochondrial perspective and therapeutic approaches. Neurological Sciences: Official Journal of the Italian Neurological Society and of the Italian Society of Clinical Neurophysiology. 2024; 45: 4121–4131. https://doi.org/10.1007/s10072-024-07508-6.

[15] Belosludtseva NV, Matveeva LA, Belosludtsev KN. Mitochondrial Dyshomeostasis as an Early Hallmark and a Therapeutic Target in Amyotrophic Lateral Sclerosis. International Journal of Molecular Sciences. 2023; 24: 16833. https://doi.org/10.3390/ijms242316833.

[16] Al-Sarraj S, King A, Cleveland M, Pradat PF, Corse A, Roth-

stein JD, *et al*. Mitochondrial abnormalities and low grade inflammation are present in the skeletal muscle of a minority of patients with amyotrophic lateral sclerosis; an observational myopathology study. Acta Neuropathologica Communications. 2014; 2: 165. https://doi.org/10.1186/s40478-014-0165-z.

[17] Tsitkanou S, Della Gatta PA, Russell AP. Skeletal Muscle Satellite Cells, Mitochondria, and MicroRNAs: Their Involvement in the Pathogenesis of ALS. Frontiers in Physiology. 2016; 7: 403. https://doi.org/10.3389/fphys.2016.00403.

[18] Song W, Song Y, Kincaid B, Bossy B, Bossy-Wetzel E. Mutant SOD1G93A triggers mitochondrial fragmentation in spinal cord motor neurons: neuroprotection by SIRT3 and PGC-1α. Neurobiology of Disease. 2013; 51: 72–81. https://doi.org/10.1016/j.nbd.2012.07.004.

[19] Zhang Y, Davis C, Sakellariou GK, Shi Y, Kayani AC, Pulliam D, *et al*. CuZnSOD gene deletion targeted to skeletal muscle leads to loss of contractile force but does not cause muscle atrophy in adult mice. FASEB Journal: Official Publication of the Federation of American Societies for Experimental Biology. 2013; 27: 3536–3548. https://doi.org/10.1096/fj.13-228130.

[20] Gurney ME, Pu H, Chiu AY, Dal Canto MC, Polchow CY, Alexander DD, *et al*. Motor neuron degeneration in mice that express a human Cu,Zn superoxide dismutase mutation. Science (New York, N.Y.). 1994; 264: 1772–1775. https://doi.org/10.1126/science.8209258.

[21] Fujisawa T, Takahashi M, Tsukamoto Y, Yamaguchi N, Nakoji M, Endo M, *et al*. The ASK1-specific inhibitors K811 and K812 prolong survival in a mouse model of amyotrophic lateral sclerosis. Human Molecular Genetics. 2016; 25: 245–253. https://doi.org/10.1093/hmg/ddv467.

[22] Acevedo-Arozena A, Kalmar B, Essa S, Ricketts T, Joyce P, Kent R, *et al*. A comprehensive assessment of the SOD1G93A low-copy transgenic mouse, which models human amyotrophic lateral sclerosis. Disease Models & Mechanisms. 2011; 4: 686–700. https://doi.org/10.1242/dmm.007237.

[23] Hatzipetros T, Kidd JD, Moreno AJ, Thompson K, Gill A, Vieira FG. A Quick Phenotypic Neurological Scoring System for Evaluating Disease Progression in the SOD1-G93A Mouse Model of ALS. Journal of Visualized Experiments: JoVE. 2015; 53257. https://doi.org/10.3791/53257.

[24] Kumar A, Accorsi A, Rhee Y, Girgenrath M. Do's and don'ts in the preparation of muscle cryosections for histological analysis. Journal of Visualized Experiments: JoVE. 2015; e52793. https://doi.org/10.3791/52793.

[25] Belosludtseva NV, Uryupina TA, Pavlik LL, Mikheeva IB, Talanov EY, Venediktova NI, *et al*. Pathological Alterations in Heart Mitochondria in a Rat Model of Isoprenaline-Induced Myocardial Injury and Their Correction with Water-Soluble Taxifolin. International Journal of Molecular Sciences. 2024; 25: 11596. https://doi.org/10.3390/ijms252111596.

[26] Frezza C, Cipolat S, Scorrano L. Organelle isolation: functional mitochondria from mouse liver, muscle and cultured fibroblasts. Nature Protocols. 2007; 2: 287–295. https://doi.org/10.1038/nprot.2006.478.

[27] Belosludtsev KN, Starinets VS, Talanov EY, Mikheeva IB, Dubinin MV, Belosludtseva NV. Alisporivir Treatment Alleviates Mitochondrial Dysfunction in the Skeletal Muscles of C57BL/6NCrl Mice with High-Fat Diet/Streptozotocin-Induced Diabetes Mellitus. International Journal of Molecular Sciences. 2021; 22: 9524. https://doi.org/10.3390/ijms22179524.

[28] Makrecka-Kuka M, Krumschnabel G, Gnaiger E. High-Resolution Respirometry for Simultaneous Measurement of Oxygen and Hydrogen Peroxide Fluxes in Permeabilized Cells, Tissue Homogenate and Isolated Mitochondria. Biomolecules. 2015; 5: 1319–1338. https://doi.org/10.3390/biom5031319.

[29] Pryor WA, Castle L. Chemical methods for the detection of lipid hydroperoxides. Methods in Enzymology. 1984; 105: 293–299. https://doi.org/10.1016/s0076-6879(84)05037-0.

[30] Chung MJ, Suh YL. Ultrastructural changes of mitochondria in the skeletal muscle of patients with amyotrophic lateral sclerosis. Ultrastructural Pathology. 2002; 26: 3–7. https://doi.org/10.1080/01913120252934260.

[31] Belosludtsev KN, Dubinin MV, Belosludtseva NV, Mironova GD. Mitochondrial Ca2+ Transport: Mechanisms, Molecular Structures, and Role in Cells. Biochemistry. Biokhimiia. 2019; 84: 593–607. https://doi.org/10.1134/S0006297919060026.

[32] Krasnianski A, Deschauer M, Neudecker S, Gellerich FN, Müller T, Schoser BG, *et al*. Mitochondrial changes in skeletal muscle in amyotrophic lateral sclerosis and other neurogenic atrophies. Brain: a Journal of Neurology. 2005; 128: 1870–1876. https://doi.org/10.1093/brain/awh540.

[33] Xiao Y, Karam C, Yi J, Zhang L, Li X, Yoon D, *et al*. ROS-related mitochondrial dysfunction in skeletal muscle of an ALS mouse model during the disease progression. Pharmacological Research. 2018; 138: 25–36. https://doi.org/10.1016/j.phrs.2018.09.008.

[34] Howard J, Chaouch A, Douglas AGL, MacLeod R, Roggenbuck J, McNeill A. Genetic testing for monogenic forms of motor neuron disease/amyotrophic lateral sclerosis in unaffected family members. European Journal of Human Genetics: EJHG. 2025; 33: 7–13. https://doi.org/10.1038/s41431-024-01718-4.

[35] Smith EF, Shaw PJ, De Vos KJ. The role of mitochondria in amyotrophic lateral sclerosis. Neuroscience Letters. 2019; 710: 132933. https://doi.org/10.1016/j.neulet.2017.06.052.

[36] Obrador E, Salvador-Palmer R, López-Blanch R, Jihad-Jebbar A, Vallés SL, Estrela JM. The Link between Oxidative Stress, Redox Status, Bioenergetics and Mitochondria in the Pathophysiology of ALS. International Journal of Molecular Sciences. 2021; 22: 6352. https://doi.org/10.3390/ijms22126352.

[37] Luo G, Yi J, Ma C, Xiao Y, Yi F, Yu T, *et al*. Defective mitochondrial dynamics is an early event in skeletal muscle of an amyotrophic lateral sclerosis mouse model. PloS One. 2013; 8: e82112. https://doi.org/10.1371/journal.pone.0082112.

[38] Vinsant S, Mansfield C, Jimenez-Moreno R, Del Gaizo Moore V, Yoshikawa M, Hampton TG, *et al*. Characterization of early pathogenesis in the SOD1(G93A) mouse model of ALS: part II, results and discussion. Brain and Behavior. 2013; 3: 431–457. https://doi.org/10.1002/brb3.142.

[39] Ciuro M, Sangiorgio M, Leanza G, Gulino R. A Meta-Analysis Study of SOD1-Mutant Mouse Models of ALS to Analyse the Determinants of Disease Onset and Progression. International Journal of Molecular Sciences. 2022; 24: 216. https://doi.org/10.3390/ijms24010216.

[40] Caldi Gomes L, Hänzelmann S, Hausmann F, Khatri R, Oller S, Parvaz M, *et al*. Multiomic ALS signatures highlight subclusters and sex differences suggesting the MAPK pathway as therapeutic target. Nature Communications. 2024; 15: 4893. https://doi.org/10.1038/s41467-024-49196-y.

[41] Méndez-López I, Sancho-Bielsa FJ, Engel T, García AG, Padín JF. Progressive Mitochondrial SOD1^{G93A} Accumulation Causes Severe Structural, Metabolic and Functional Aberrations through OPA1 Down-Regulation in a Mouse Model of Amyotrophic Lateral Sclerosis. International Journal of Molecular Sciences. 2021; 22: 8194. https://doi.org/10.3390/ijms22158194.

[42] Liu YJ, Lee LM, Lai HL, Chern Y. Aberrant activation of AMP-activated protein kinase contributes to the abnormal distribution of HuR in amyotrophic lateral sclerosis. FEBS Letters. 2015; 589: 432–439. https://doi.org/10.1016/j.febslet.2014.12.029.

[43] Liu YJ, Tsai PY, Chern Y. Energy Homeostasis and Abnormal RNA Metabolism in Amyotrophic Lateral Sclerosis. Frontiers in Cellular Neuroscience. 2017; 11: 126. https://doi.org/10.3389/

fncel.2017.00126.
[44] Lippe G, Comelli M, Mazzilis D, Sala FD, Mavelli I. The inactivation of mitochondrial F1 ATPase by H2O2 is mediated by iron ions not tightly bound in the protein. Biochemical and Biophysical Research Communications. 1991; 181: 764–770. https://doi.org/10.1016/0006-291x(91)91256-c.
[45] Okoye CN, Koren SA, Wojtovich AP. Mitochondrial complex I ROS production and redox signaling in hypoxia. Redox Biology. 2023; 67: 102926. https://doi.org/10.1016/j.redox.2023.102926.
[46] Echaniz-Laguna A, Zoll J, Ribera F, Tranchant C, Warter JM, Lonsdorfer J, *et al*. Mitochondrial respiratory chain function in skeletal muscle of ALS patients. Annals of Neurology. 2002; 52: 623–627. https://doi.org/10.1002/ana.10357.
[47] Fayemendy P, Marin B, Labrunie A, Boirie Y, Walrand S, Achamrah N, *et al*. Hypermetabolism is a reality in amyotrophic lateral sclerosis compared to healthy subjects. Journal of the Neurological Sciences. 2021; 420: 117257. https://doi.org/10.1016/j.jns.2020.117257.
[48] Rogers RS, Tungtur S, Tanaka T, Nadeau LL, Badawi Y, Wang H, *et al*. Impaired Mitophagy Plays a Role in Denervation of Neuromuscular Junctions in ALS Mice. Frontiers in Neuroscience. 2017; 11: 473. https://doi.org/10.3389/fnins.2017.00473.
[49] Tak YJ, Park JH, Rhim H, Kang S. ALS-Related Mutant SOD1 Aggregates Interfere with Mitophagy by Sequestering the Autophagy Receptor Optineurin. International Journal of Molecular Sciences. 2020; 21: 7525. https://doi.org/10.3390/ijms21207525.
[50] Da Cruz S, Parone PA, Lopes VS, Lillo C, McAlonis-Downes M, Lee SK, *et al*. Elevated PGC-1α activity sustains mitochondrial biogenesis and muscle function without extending survival in a mouse model of inherited ALS. Cell Metabolism. 2012; 15: 778–786. https://doi.org/10.1016/j.cmet.2012.03.019.
[51] Gao FB, Almeida S, Lopez-Gonzalez R. Dysregulated molecular pathways in amyotrophic lateral sclerosis-frontotemporal dementia spectrum disorder. The EMBO Journal. 2017; 36: 2931–2950. https://doi.org/10.15252/embj.201797568.
[52] Guo Y, Zhang Y, Wen D, Duan W, An T, Shi P, *et al*. The modest impact of transcription factor Nrf2 on the course of disease in an ALS animal model. Laboratory Investigation; a Journal of Technical Methods and Pathology. 2013; 93: 825–833. https://doi.org/10.1038/labinvest.2013.73.
[53] Nishimune H, Stanford KG, Chen J, Odum JD, Rorie AD, Rogers RS, *et al*. Forelimb Resistance Exercise Protects Against Neuromuscular Junction Denervation in the SOD1-G93A Rat Model of ALS. Degenerative Neurological and Neuromuscular Disease. 2022; 12: 145–155. https://doi.org/10.2147/DNND.S388455.
[54] Kook MG, Lee S, Shin N, Kong D, Kim DH, Kim MS, *et al*. Repeated intramuscular transplantations of hUCB-MSCs improves motor function and survival in the SOD1 $G^{93}A$ mice through activation of AMPK. Scientific Reports. 2020; 10: 1572. https://doi.org/10.1038/s41598-020-58221-1.
[55] Angelova PR, Abramov AY. Functional role of mitochondrial reactive oxygen species in physiology. Free Radical Biology & Medicine. 2016; 100: 81–85. https://doi.org/10.1016/j.freeradbiomed.2016.06.005.
[56] Baev AY, Vinokurov AY, Potapova EV, Dunaev AV, Angelova PR, Abramov AY. Mitochondrial Permeability Transition, Cell Death and Neurodegeneration. Cells. 2024; 13: 648. https://doi.org/10.3390/cells13070648.
[57] Yu CH, Davidson S, Harapas CR, Hilton JB, Mlodzianoski MJ, Laohamonthonkul P, *et al*. TDP-43 Triggers Mitochondrial DNA Release via mPTP to Activate cGAS/STING in ALS. Cell. 2020; 183: 636–649.e18. https://doi.org/10.1016/j.cell.2020.09.020.
[58] Scaricamazza S, Salvatori I, Amadio S, Nesci V, Torcinaro A, Giacovazzo G, *et al*. Repurposing of Trimetazidine for amyotrophic lateral sclerosis: A study in $SOD1^{G93A}$ mice. British Journal of Pharmacology. 2022; 179: 1732–1752. https://doi.org/10.1111/bph.15738.